Pure hydrogen production by steam-iron process: the synergic effect of MnO_2 and Fe_2O_3

[1] Paolo De Filippis, [2] Livio D'Alvia, [1]* Martina Damizia, [1] Benedetta de Caprariis, [2] Zaccaria Del Prete

[1] SAPIENZA University of Rome, Department of Chemical Engineering Materials Environment, Via Eudossiana 18, 00184 Rome, Italy.
[2] SAPIENZA University of Rome, Department of Mechanical and Aerospace Engineering, Via Eudossiana 18, 00184 Rome, Italy

*Corresponding author. Tel.: +3906 44585566; Fax: +3906 4827453.
e-mail address: martina.damizia@uniroma1.it

ABSTRACT

In the energy transition from fossil to clean fuels, hydrogen plays a key role. Proton-exchange membrane fuel cells (PEMFCs) represent the most promising hydrogen application, but they require a pure hydrogen stream (CO < 10 ppm). The steam iron process represents a technology for the production of pure H_2, exploiting iron redox cycles. If renewable reducing agents are used, the process can be considered completely green. In this context, bio-ethanol can be an interesting solution that is still not thoroughly explored. In this work, the use of ethanol as a reducing agent in the steam iron process will be investigated. Ethanol at high temperature decomposes mainly in syngas but can also form coke, which can compromise the process effectiveness, reacting with water and producing CO together with H_2. In this work, the coke deposition is avoided controlling the duration of the reduction step; in fact, the data demonstrated that coke deposition is significantly dependent on reduction time. Tests were carried out in a fixed bed reactor using hematite (Fe_2O_3) as raw iron oxide adopting several reduction time (7 min – 25 min). The effect of the addition of MnO_2 to increase the reduction degree of iron oxides was explored using different amount of MnO_2 (10 wt% and 40 wt% with respect to Fe_2O_3). The hypothesis is that MnO_2, due to its high oxygen mobility, promotes the decomposition of ethanol in syngas, enhancing the methane cracking by oxidizing the coke formed in this reaction. The tests were performed at fixed temperatures of 675 °C and atmospheric pressure. The optimization of the reduction time in the chosen operating condition performed only with Fe_2O_3 shows that feeding an amount of 5 $mmol_{C2H5OH}/g_{Fe2O3}$ coke deposition is avoided and therefore a pure H_2 stream in oxidation is obtained. The addition of MnO_2 leads to increased H_2 yield and process efficiency confirming its positive effect on the reduction degree of the solid bed. A reaction pathway to demonstrate the synergic effect of Fe_2O_3 and MnO_2 in the reduction step was proposed in this article.

Keywords: Hydrogen, steam-iron process, manganese oxides, bioethanol, chemical looping, efficiency measurement.

1. INTRODUCTION

In recent years the number of applications that require carbon monoxide-free hydrogen is significantly increasing [1,2]. Among these, a major boost was given by the development of proton-exchange membrane fuel cells (PEMFCs) considered as an essential element in the transition from fossil fuels to cleaner forms of mobility [3]. Nowadays, if pure hydrogen is supplied, electricity can be produced without polluting emissions, helping to solve the problem of global warming [4].

However, the use of hydrogen to produce energy shows two critical limitations. It is not present in nature and it can be produced only using other primary sources such as organic compounds with high H/C molar ratio and water [5]. Traditional hydrogen production technologies such as steam reforming, partial oxidation and autothermal reforming, which count for 95% of the total hydrogen industry, have the main disadvantages to use fossil sources as raw material and to require complexes and expensive purification systems [6]. To support

a sustainable hydrogen economy, it is essential to link hydrogen production to renewable sources [7,8]; this goal is aimed at reducing the anthropogenic CO_2 emissions due to fossil fuel utilization and the high cost associated with hydrogen production technologies. Nowadays, at industrial scale, the production of pure hydrogen from renewable sources is possible only with water electrolysis. This process uses electricity to split water into hydrogen and oxygen [9]. However, since electrolysis cost is stronglhy related to purchase price of the electicity during the operating period, its application is limited [10].

Among the processes to produce hydrogen from renewable sources, chemical-looping hydrogen (CLH) seems to be one of the most attractive technologies to obtain a pure hydrogen stream. This technology exploits the ability of some metals to be oxidized and reduced cyclically, keeping constant their activity for a high number of redox cycles [11,12]. Syngas, produced by both fossil and renewable sources [13], was often used as a reducing agent while the production of pure hydrogen occurs in the subsequent step of oxidation with steam. Transition metals such as Cu, Cd, Ni, Mn, Fe and Co are characterized by different available oxidation states, which give them excellent redox properties. The majority of these metals have already been successfully tested as solid oxygen carrier into chemical looping combustion (CLC) systems. CLC is a promising combustion technology that guarantees a high process efficiency, ensuring the possibility of capturing CO_2. A pure CO_2 stream easy to be capture and stored can be obtained using transition metals oxides as solid oxygen carrier which are able to supply the oxygen necessary to burn the fuel without using air. Subsequently, the metal oxides are restored, feeding air to the reactor. Nickel oxide is reported to be the most reactive and stable material for a high number of redox cycles. However, extensive studies are conducted to research an alternative solid oxygen carrier due to the well-known toxicity of Ni. Based on the promising results obtained with chemical looping combustion, CLH is widely studied in the hydrogen production field.

Thanks to its high reactivity in redox reactions, low cost and environmentally friendly nature, iron is one of the most used metals in CLH processes called, in this case, the steam iron process. Voitic et al. [14] discussed the activity of $Fe_2O_3/Al_2O_3/CeO_2$ catalyst in a high-pressure steam-iron process (50 atm) using syngas as a reducing agent and they obtained H_2 with a purity of 99.98%. Chiesa et al. [15] proposed a chemical looping system constituted by three rectors, one for the reduction step, one for the oxidation with steam and the last for the oxidation with air. The air oxidation is performed to sustain the thermal balance of the process, oxidizing Fe3O4 again to Fe2O3.

Hormilleja et al. [16] and Yang et al. [17] reduced iron-based solid material with ethanol and coal char, respectively, producing in both case H_2 suitable for any type of fuel cell. Bleeker et al. [18] explored the use of pyrolysis oil gasification to reduce iron oxides obtaining in the oxidation step a hydrogen amount equal to 840 NL/kg $_{dry}$ $_{pyrolysis\ oil}$ accompanied by 7 NL/kg $_{dry\ pyrolysis\ oil}$ of carbon-based compounds. Gupta et al. [19] evaluated Ni, Cu, Cd, Co, Mn, Sn and Fe oxides for the CLH process based on thermodynamic equilibrium limitations. The study found that Fe_2O_3 provided the best conversion of syngas to combustion products of CO_2 and H_2O, along with the high conversion of steam to hydrogen. Li et al. [20] selected several metal oxides to be used as oxygen carriers in the chemical looping hydrogen process. They found that iron oxide is the best choice considering overall properties, including oxygen-carrying capacity, thermodynamic properties, reaction kinetics, physical strength, melting points, and environmental effects. Urasaki et al. [21] investigated hydrogen production by the steam iron reaction using iron oxide modified with minimal amounts of palladium or zirconia (0.23 mol%) at a temperature of 450 °C and under atmospheric pressure. Their addition enhanced the H_2 yields suppressing the synthetization of the iron particles. Jin et al. [22] tested (NiO: Fe_2O_3)/bentonite particles as the best mediator for the chemical-looping hydrogen generation system to achieve stable continuous operation. Galvita et al. [23] found that the addition of Ce could inhibit the sintering of the iron oxide.

The use of ethanol in hydrogen production is widely explored thanks to its low cost and its renewable nature. Ethanol is a linear alcohol widely produced by biomass fermentation of sugar, starch and organic waste [24]. Besides, at room temperature, it is stable in liquid form and, therefore, easy to store and transport. Currently, thanks to these excellent properties and its high calorific value, it is also used as renewable fuel [25]. Ethanol at high temperature and ambient pressure is decomposed into a gaseous mixture mainly constituted by H_2 and CO, having high reducing power. Although the ethanol decomposition pathway is the focus of many

studies in the H_2 production field, the complex system of reactions occurring is still not clear and therefore, its use is in the experimental phase [26,27].

In this work, the steam iron process was studied in order to produce a pure hydrogen stream to be supplied in a PEM fuel cell sustainably, starting from Fe_2O_3 powder as raw iron oxide and ethanol as a reducing agent. To obtain pure hydrogen, the optimization of the operative conditions is fundamental: several reduction times of the Fe_2O_3 bed were explored, and the addition of MnO_2 to increase the process efficiency was studied. The hypothesis is that MnO_2 can improve the degree of reduction of the solid bed, increasing reducing species in the ethanol decomposition gas stream and, therefore, enhance the process efficiency[28]. Manganese Oxides (MnO_x) are widely used in many studies as a catalyst in oxidation reactions, especially combustion [29,30]. Manganese, like iron, has several oxidation states and excellent redox properties, and thus it is also a perfect candidate to be coupled with iron in the hydrogen production [31,32]. The combination of iron/manganese oxides as solid oxygen carrier is already successfully explored into CLC systems, and generally, the presence of manganese oxides promotes the fuel combustion efficiency. For example, Miller D. D. et al. [33] reported that the addition of MnO_2 on Fe based oxygen carried led to a higher oxygen transfer capacity at 900 °C using methane as fuel.

However, to the best of our knowledge, no studies have been conducted coupling MnO_2 and Fe_2O_3 in the steam iron process. In this study thus the aim is to evaluate if the high redox reactivity of the Mn/Fe oxides system reported in the CLC processes can also be exploited in the steam iron process using bio-ethanol in the reduction step. The effect of MnO_2 addition in the process efficiency is investigated, focusing the attention on the degree of reduction of iron oxide and thus on the amount of hydrogen produced.

1.1 IRON AND MANGANESE REDOX SYSTEM WITH SYNGAS

The mechanism of the reduction process from Fe_2O_3 to metallic iron is not trivial since iron has different oxidation states and can produce many oxides such as hematite (Fe_2O_3), magnetite (Fe_3O_4) and wustite (FeO). Furthermore, the composition of the gas stream produced from ethanol decomposition is not well defined; we know that the species having a higher concentration are CO and H_2, which are considered in this work the two principal reducing agents. At the operating condition adopted, the reduction is divided into three steps:

1° step

$3Fe_2O_3 + H_2 \leftrightarrow 2Fe_3O_4 + H_2O$	ΔH= -12.175 kJ/mol	(1)
$3Fe_2O_3 + CO \leftrightarrow 2Fe_3O_4 + CO_2$	ΔH= -47.09 kJ/mol	(2)

2° step

$Fe_3O_4 + H_2 \leftrightarrow 3FeO + H_2O$	ΔH= +50.61 kJ/mol	(3)
$Fe_3O_4 + CO \leftrightarrow 3FeO + CO_2$	ΔH= +15.70 kJ/mol	(4)

3° step

$FeO + H_2 \leftrightarrow Fe + H_2O$	ΔH= +15.03 kJ/mol	(5)
$FeO + CO \leftrightarrow Fe + CO_2$	ΔH= -19.88 kJ/mol	(6)

First, Fe_2O_3 is reduced to Fe_3O_4 (equations 1 and 2), then Fe_3O_4 is reduced to FeO (equations 3 and 4); finally, the complete reduction to metallic iron is achieved (equations 5 and 6) [34].

After the reduction phase, the oxidation step occurs in the presence of water vapor and the restored iron oxide is Fe_3O_4 (equation 7). The oxidation of Fe_3O_4 to Fe_2O_3 with water vapor is thermodynamically not favored (ΔG>0), and to restore the initial iron oxide (Fe_2O_3), the use of air or oxygen is necessary [18]. The obtained Fe_3O_4 can be reduced again in a subsequent reduction step, thus guaranteeing the cyclical nature of the process. In this step, pure hydrogen is produced.

$$3Fe + 4H_2O \leftrightarrow Fe_3O_4 + 4H_2 \qquad\qquad \Delta H= \text{-95,646 kJ/mol} \qquad\qquad (7)$$

MnO_2 powder addition has the aim of improving the degree of reduction of iron oxides in order to increase the hydrogen yields, knowing that, as reported in various studies, MnO_x participates in the redox reaction system [32,35]. MnO_2 can also be reduced to MnO in three steps: first, MnO_2 is reduced to Mn_2O_3 according to the equation 8 and 9, then Mn_2O_3 is reduced to Mn_3O_4 (equation 10-11) which is finally reduced to MnO (equations 12 and 13). The complete reduction to Mn cannot be achieved under the operating conditions adopted $(\Delta G>0)$[35].

1° step
$$2MnO_2 + H_2 \leftrightarrow Mn_2O_3 + H_2O \qquad\qquad (8)$$
$$2MnO_2 + CO \leftrightarrow Mn_2O_3 + CO_2 \qquad\qquad (9)$$
2° step
$$3Mn_2O_3 + H_2 \leftrightarrow 2Mn_3O_4 + H_2O \qquad\qquad (10)$$
$$3Mn_2O_3 + CO \leftrightarrow 2Mn_3O_4 + CO_2 \qquad\qquad (11)$$
3° step
$$Mn_3O_4 + H_2 \leftrightarrow 3MnO + H_2O \qquad\qquad (12)$$
$$Mn_3O_4 + CO \leftrightarrow 3MnO + CO_2 \qquad\qquad (13)$$

In the oxidation phase MnO, in the presence of water vapor, can be oxidized to Mn_2O_3, releasing H_2 according to equation 14. The oxide obtained is Mn_2O_3, since to restore MnO_2, at the temperatures used, pressures higher than 3000 atm are necessary [32].

$$2MnO + H_2O \leftrightarrow Mn_2O_3 + H_2 \qquad\qquad (14)$$

Therefore, MnO_2 plays a dual role in the steam iron process: it enhances the reduction of the iron oxides in the reduction phase and participates as active specie in the H_2 production in the oxidation step. A simplified illustration of the proposed system is reported in figure 1.
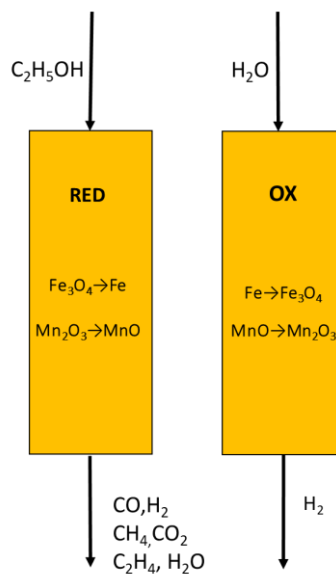
Fig. 1: Steam-iron process in a fixed bed reactor using C_2H_5OH as a reducing agent and a mixture of Fe_2O_3 and MnO_2 powders as a solid bed.

2. EXPERIMENTAL SETUP

The experiments were conducted in a fixed-bed reactor (stainless steel, ID 9 mm, length 300 mm) heated by an external electric heater at a constant temperature of 675 °C. Both the reduction and oxidation steps were conducted at ambient pressure. The solid bed is constituted by a powder mixture of Fe_2O_3 (assay ≥ 99%, particle size < 5 μm, provided by Sigma-Aldrich), silicon dioxide SiO_2 (assay ≥ 99.9%, particle size ≤ 74 μm, provided by Sigma-Aldrich) and manganese dioxide MnO_2 (assay = 99.9%, particle size < 10 μm, provided by Sigma-Aldrich). SiO_2 was added to avoid iron particles agglomeration and to uniform temperature profile in the bed. All tests were performed with a constant carrier gas flowrate (Argon flowrate = 120 mL/min). The pressure drops of the reactor were measured by an electronic manometer (Druck-DP260 equipped with a pressure transmitter DPR 910). Due to the size of the used powders, a slight increase in the reactor pressure is detected (0.05 atm). However, considering the use of the particles in the form of powder and comparing the pressure drop relieved with the typical values available in the literature for fixed bed reactor [36], the pressure drops are considered negligible.

Ethanol and water flowrates were set to 4 mL/h and fed at the top of the reactor by a syringe pump (KD Scientific); before entering into the reactor, both ethanol and water are vaporized in an evaporator heated at 230 °C. In a typical test, 1,59 g of Fe_2O_3 and 0.53 g of SiO_2 were used, while in the experiments with MnO_2, an amount of powder of 10 wt% and 40 wt% to Fe_2O_3 was added. Blank experiments were performed feeding ethanol and argon on a solid bed constituted by only the unreactive SiO_2. The ethanol flow rate was kept constant and equal to that used in steam iron tests. The amount of SiO_2 loaded is equal to the amount of hematite used in the steam iron experiments.

In the reduction phase, three different ethanol feeding times were considered 25, 9 and 7 minutes, while in the oxidation phase, distilled water was fed until complete oxidation of the solid bed particles. Between the reduction and oxidation phase, only argon was fed to the reactor to remove all carbon-based compounds produced in the reduction step.

Liquid products were separated by condensation and analyzed through GC-MS (Agilent 5973) and the gas composition was determined with an on-line mass spectrometer (Hiden QGA, Quantitative Gas Analyser) calibrated with a tailored standard gas mixture (gas cylinder by Sapio group). The used instrument measures H_2, CO_2, CO, CH_4, C_2H_4 and Ar concentrations in terms of molar percentage.

A non-dispersive infrared sensor (Ambra Sistemi, Comet 0005-14-312) calibrated with a tailored standard mixture (gas cylinder by Sapio group) was also used to measure the CO content in the oxidation step to ensure the concentration values were less than 10 ppm, an amount required for PEMFC application. In order to understand the mechanism of ethanol decomposition, before the steam iron tests, the blank experiments were conducted feeding only ethanol at 675 °C for 2 h loading the reactor with only SiO_2.

At least three redox cycles were considered in each test.

Figure 2 shows a simplified scheme of the laboratory plant used.
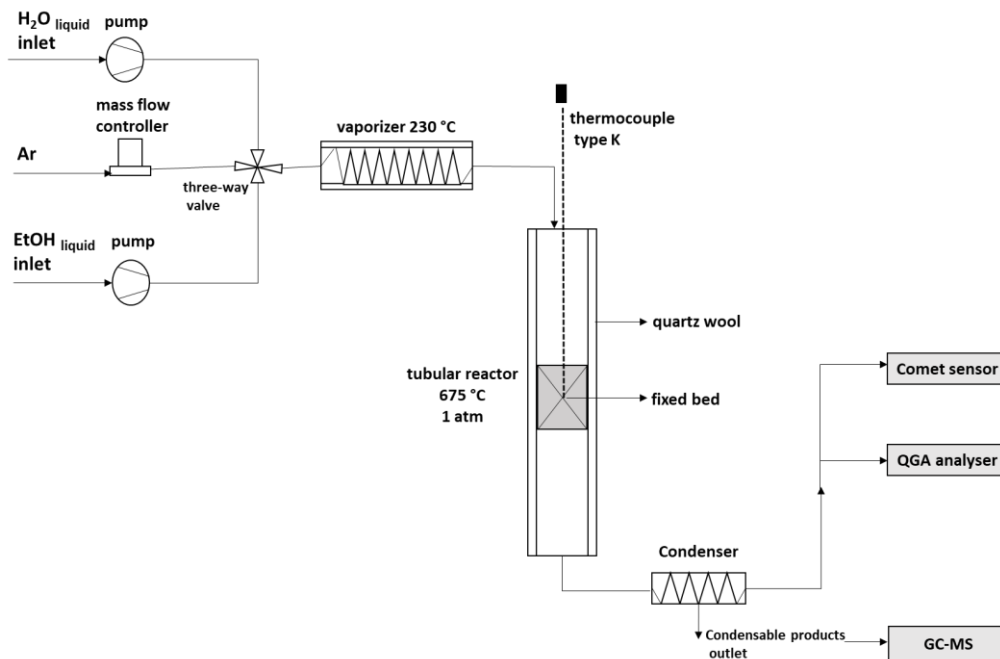
Fig. 2: Schematic process diagram adopted for the experimental tests.

3. RESULTS AND DISCUSSION

3.1 THERMAL ETHANOL DECOMPOSITION

At the operating conditions adopted in the reduction step (675 °C and 1 atm), ethanol participates in a complex system of reactions that are difficult to identify. In order to evaluate the main compounds resulting from its thermal decomposition and the feasibility to use it as a source of reducing gasses (H_2 and CO), a blank experiment was carried out.

The several compounds resulting from ethanol decomposition are grouped based on their physical state (gas, liquid and solid) to understand the influence of the different reactions in which ethanol can participates.

The typical molar composition of the gaseous mixture produced as a function of time is reported in figure 3 while the carbon balance and the yields of each phase (gas, liquid and solid) are reported in table 1 and table 2, respectively.
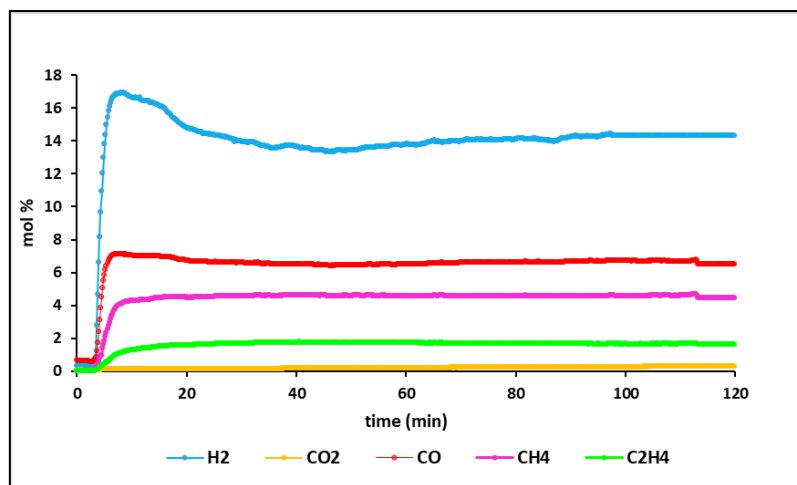

Fig.3 Molar concentration of the principal gaseous compounds resulted from thermal ethanol decomposition at 675 °C and 1 atm.

As shown in figure 3, a gaseous mixture mainly constituted by H_2 (15.06%), CO (7.13%), CH_4 (4.51%) and by traces of C_2H_4 (1.73%) and CO_2 (0.22%) is produced from thermal ethanol decomposition. The equilibrium values obtained by Gibbs free energy minimization at the same operative conditions (675 °C and 1 atm) were also calculated. At equilibrium, the molar gas composition is H_2 (24.04%), CO (8.64%), CH_4 (0.94%); ethanol results to be entirely converted and CO_2 and ethylene are not present. The results of the equilibrium calculation are very similar to those of experimental ones confirming the thermodynamic feasibility to produce a high-reductive stream mainly constituted by H_2 and CO from ethanol. The concentration of each species remains constant throughout the test. This result confirms that ethanol can be successfully used as a source of reducing agent in the proposed system.

At the end of the test, the condensable products were collected, weighted and finally analyzed; from GC-MS analysis, only water is detected in the condensate, suggesting that ethanol is completely converted. Traces of carbon deposits on the silica bed were also relived. The amount of coke produced in the blank experiments was quantified by controlled combustion with air in a muffle furnace. All samples are heated at 600 °C for 2 hours, to perform the complete conversion of carbon. The difference of the sample weight permits to calculate the amount of carbon before and after the combustion treatment.

Table 1 shows the carbon balance of the reactor calculated considering all the three phases (gas, liquid and solid) produced. The calculation confirmed the validity of the results, although a difference of 0.87% between the input and output carbon moles was identified; nevertheless, being this deviation within the error range of the instrument, it is considered negligible.

Table 1: Carbon balance for thermal ethanol decomposition experiments at 675 °C and 1 atm pressure.

	IN	OUT			
	C_2H_5OH	Gas	Liquid	Solid	Δ
mol C*	0.274	0.237±0.001	0.000	0.028±0.002	0.009 mol C
% mol C	100.00	86.86±0.10	0.000	10.34± 0.15	2.8 % mol C

* The measurements are repeated three times; dispersion evaluates through semi-dispersion.

Where:

mol C $_{C2H5OH}$ = total mols of carbon fed with ethanol;

% mol C $_{Gas}$ = 100*mols of carbon in the gaseous compounds/mol C $_{C2H5OH}$;

% mol C $_{liquid}$ = 100*mols of carbon in the condensable products/ mol C $_{C2H5OH}$;

% mol C $_{solid}$ = 100*mols of coke on the SiO_2 bed/ mol C $_{C2H5OH}$;

Δmol C = mol C $_{C2H5OH}$ - sum of mol C products

Table 2 shows the gas, liquid and solid yields obtained from ethanol decomposition (molar basis). These data are reported to understand better what is the predominant phase in which ethanol is decomposed. As desired, looking at the results in table 2, ethanol is principally converted into gaseous products (95.13 mol%). At the same time, condensable (H_2O) and solid compounds (coke) are obtained only in a very low amount (0.86 mol% and 4.05 mol%, respectively) and can be considered by-products. However, despite the low coke yield detected (4.05 mol%), to use ethanol in this technology, the reactions leading to coke formation should be totally inhibited.

Table 2: Molar yields of products resulting from thermal ethanol decomposition at 675°C and 1 atm pressure.

	C_2H_5OH $_{in}$	Products	Gas	Liquid	Solid
mol*	0.137	0.698 ± 0.011	0.664 ± 0.010	0.006 ± 0.001	0.028 ± 0.001
Yield (mol%)	0.00	100.00 ± 1.10	95.13 ± 1.01	0.86 ± 0.05	4.05 ± 0.15

* The measurements are repeated three times; dispersion evaluates through semi-dispersion.

Where:

mol $_{C2H5OH}$ = total mols of ethanol fed;

mol $_{products}$ = total mols of products obtained;

Gas Yield (mol%) = 100*sum of the mol of gaseous products/ mol $_{products}$;

Liquid Yield (mol%) = 100* mols of water/ mol $_{products}$;

Solid Yield (mol%)= 100* mols of coke / mol $_{products}$;

Based on the results obtained and considering the mechanisms proposed in the literature, a simplified thermal decomposition scheme is reported. At the operating condition adopted in this work (675 °C and 1 atm), ethanol starts to decompose mainly in H_2, CO and CH_4, according to equation 15 [37]. However, ethanol also undergoes in dehydration reaction producing ethylene (equation 16) and water, although with low yields. Furthermore, due to the high-temperature, methane undergoes to cracking reaction (equation 17), producing additional H_2 and carbon deposits[38,39].

$$CH_3CH_2OH \leftrightarrow CO + H_2 + CH_4 \qquad \Delta H= +49 \text{ kJ/mol} \qquad (15)$$

$$CH_3CH_2OH \leftrightarrow C_2H_4 + H_2O \qquad \Delta H= +45 \text{ kJ/mol} \qquad (16)$$

$$CH_4 \leftrightarrow C+2H_2 \qquad \Delta H= +74 \text{ kJ/mol} \qquad (17)$$

Several studies about the use of ethanol about hydrogen production technologies report two additional reactions which can be responsible for the coke formation[40,41] :

$$2CO \leftrightarrow CO_2+C \qquad \Delta H= -173 \text{ kJ/mol} \qquad (18)$$

$$C_2H_4 \rightarrow \text{carbonaceous polymeric compounds (coke)} \qquad (19)$$

The proposed set of equations, except for the Boudouard reaction (equation 18), are all endothermic reactions, and thus thermodynamically favored at high temperatures. Therefore, it is worth underlining that, at the high temperatures adopted, the conversion of CO into carbon according to Boudouard reaction is thermodynamically less favored.

$$C +H_2O \leftrightarrow CO+H_2 \qquad \Delta H= +131 \text{ kJ/mol} \qquad (20)$$

$$CO+H_2O \leftrightarrow CO_2+ H_2 \qquad \Delta H= -41 \text{ kJ/mol} \qquad (21)$$

3.2 DETERMINATION OF THE OPTIMAL REDUCTION TIME OF IRON OXIDES

In order to make possible the use of ethanol in this process, the study of the operating conditions that inhibit coke formation during the reduction step is essential. For this purpose, tests at different reduction time, ranging from 7 to 25 minutes, for one redox cycle and in the presence of Fe_2O_3 were performed. Figure 4 reports the flow rate of the analyzed species: the first peak regards the reduction step, while the second the oxidation step. The results of the blank tests already shown in Fig.3 were also added in Fig.4 to better understand the behavior of the process in the presence of the iron oxide.
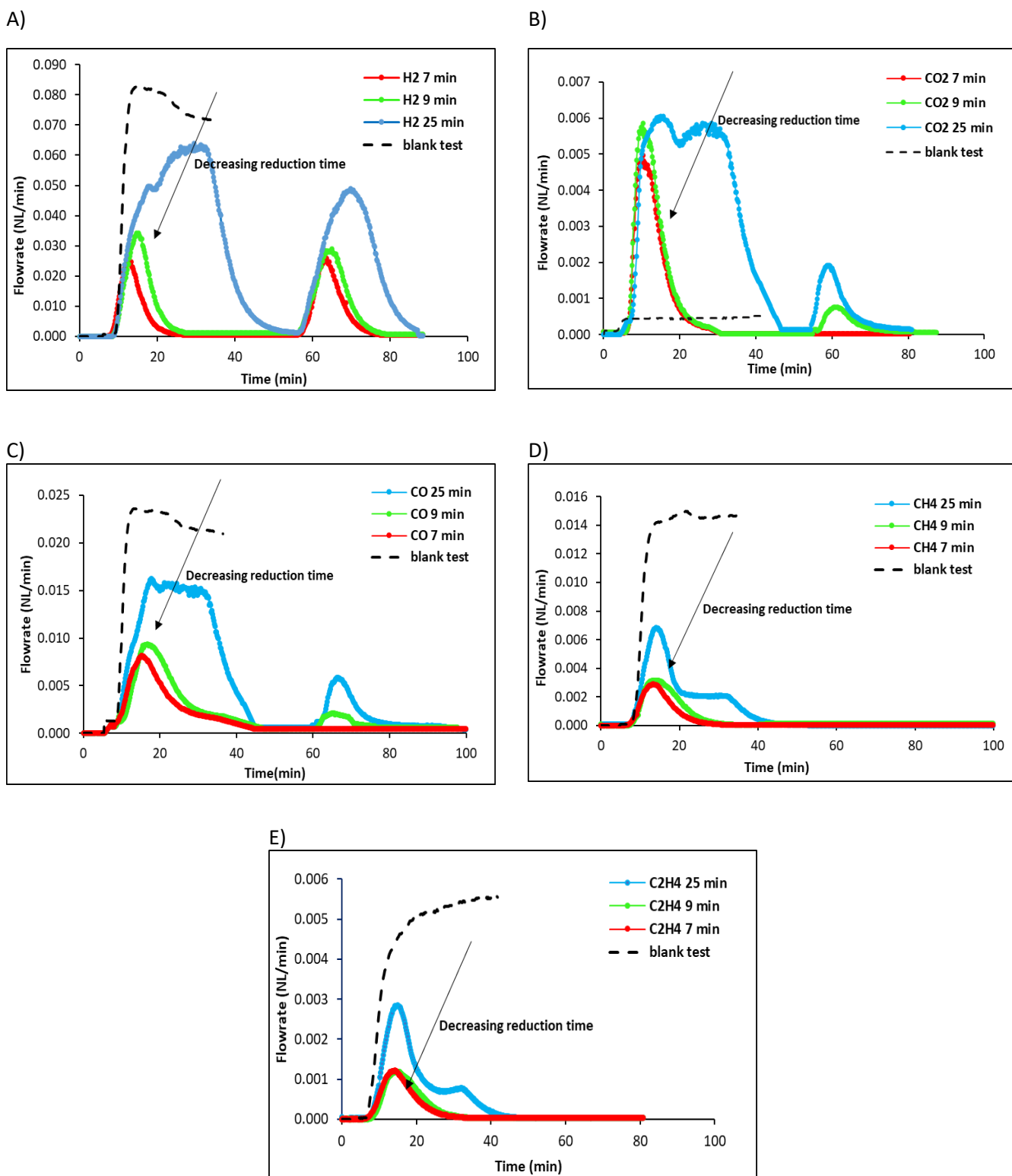
A)

B)

C)

D)

E)

Fig.4: Trend of the flow rate of the main compounds produced during one redox cycle in the presence of Fe_2O_3 at different reduction time, comparison with a blank test (dashed line). A) H_2; B) CO_2; C) CO; D) CH_4; E) C_2H_4.

Except for CO_2, all the species obtained have lower flow rates than those detected in the thermal ethanol decomposition on SiO_2; the decrease of CH_4 and C_2H_4 suggests that using ethanol, the traditional redox

system proposed with the utilization of syngas, is not enough to fully represent the iron oxides reduction. Looking at figures 4 D and 4 E, not only H_2 and CO but also CH_4 and C_2H_4 actively participate in the reduction process, being their flow rates much lower with respect to the results of the blank test. Furthermore, for a reduction time of 25 minutes, it can be noticed that CH_4 and C_2H_4 present a peculiar flow rate trend as a function of time, showing a shoulder for times higher than 15 minutes. At these reduction times, CH_4 and C_2H_4 cracking reactions are catalyzed by Fe^0 particles being produced during the reduction, leading to the formation of additional H_2 and active carbon (equation 17). The produced carbon in close contact with iron oxides can act as an additional iron reducing agent producing CO. CO can reduce again iron oxide producing more Fe and CO_2. When the complete reduction of iron oxides to Fe^0 has been reached, the formed carbon is not consumed anymore. Thus it begins to be deposited on the bed particles, inhibiting CH4 and C2H4 cracking reactions. This behavior is visible in the flow rate curves of CH4 and C2H4 concentrations, which are stabilized to a constant value. The output amounts of CO and CO_2 are, at this point, regulated by methane cracking and Boudouard equilibrium reactions.

Furthermore, when the times are higher than 15 minutes, a clear increase of H_2 and CO_2 is measured (figure 4 A and figure 4 B) while CO slowly decreases over time (figure 4 C). These results suggest that the consumption of CH_4 and C_2H_4 is strongly related to the degree of the solid bed reduction and, in particular, to the Fe^0 formation. The catalytic activity of metallic iron on the CH_4 cracking reaction is analyzed in different studies in which a complete CH_4 conversion into pure H_2 and carbon is achieved already at a temperature of 700 °C [42,43].

A simplified reaction scheme of the discussed mechanism for the reduction of iron oxides with ethanol is proposed (figure 5).
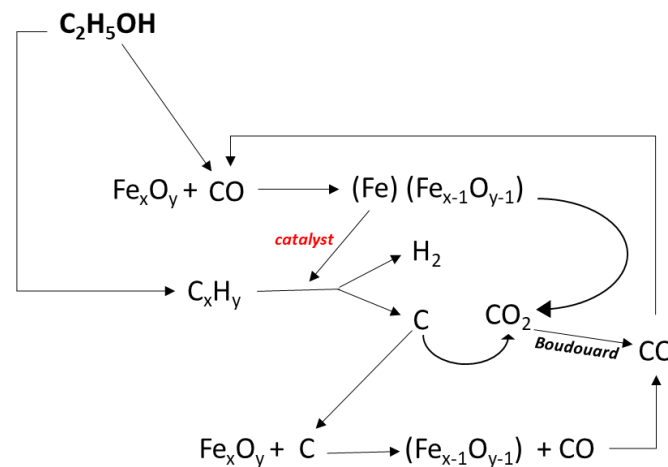

Fig 5: Mechanism proposed by CO iron oxides reduction using ethanol (675 °C, 1 atm).

Looking at the oxidation peaks reported in figure 4, it can be noted that pure hydrogen is obtained only for reduction times of 7 minutes. This result suggests that the reduction time parameter significantly influences the composition of the gas mixture due to the occurrence of the coke formation for higher reduction times. When a reduction time equal to 25 minutes and 9 minutes is used, an increase of CO_2 and CO flowrate is registered; the presence of carbonaceous compounds in the oxidation step points out that coke deposition occurred during the reduction phase is in this step gasified (equation 20). However, using a reduction time equal to 7 minutes lets to avoid carbon deposition on iron particles, but at the expense of less H_2 production. This low H_2 amount is undoubtedly due to the worse reduction degree of hematite as time decreases. However, only through an inferior reduction of the solid bed it is possible to obtain a pure flow of H_2 in the oxidation phase and, therefore to make possible the use of ethanol to produce H_2 as a feed for fuel cells.

Table 3 summarizes the volume of species obtained during the oxidation step for the three times of reduction and the efficiency of the process calculated according to equation 22, where H_{2e} is the hydrogen measured from the experimental tests and H_{2t} is the theoretical value.

$$E\ (\%) = (H_{2e} / H_{2t}) * 100 \qquad\qquad\qquad (22)$$

H_{2t} was calculated, hypothesizing that the whole amount of Fe_2O_3 loaded was reduced to metallic iron in the reduction step and then totally oxidized to Fe_3O_4 in the presence of steam. The volumes of the several species produced in each test are calculated by integrating the peaks shown in Figure 4.

The results collected in table 3 confirm that, when reduction times of 25 minutes and 9 minutes are used, carbon deposition occurs. This behavior is also confirmed by the amount of the experimental hydrogen produced, which exceeds by 4.4% the theoretical maximum hydrogen value (H_{2tv}=0.595 L) at a reduction duration of 25 minutes. Decreasing the reduction time to 7 allows the production of pure H_2 during the oxidation step, meaning that coke deposition is negligible. However, hydrogen production was significantly lower than the theoretical value (process efficiency of 39.33%) since a period of 7 minutes is not enough to achieve the complete reduction of Fe_2O_3 particles. Considering the adopted operating conditions and the amount of Fe_2O_3 added, coke deposition is avoided feeding 5 $mmol_{C2H5OH}/g_{Fe2O3}$.

Table 3: Amount of species produced during the first oxidation peak at the operating condition of 675 °C, 1 atm and different reduction time (25 min, 9 min and 7 min).

t_{red} (min)	H_{2e} (NL)	CO (NL)	CO_2 (NL)	E%
25*	0.621 ± 0.005	0.058 ± 0.004	0.015 ± 0.003	104.40 ± 0.50
9*	0.257 ± 0.005	0.029 ± 0.012	0.007 ± 0.010	43.86 ± 0.50
7§	0.210 ± 0.069	0.000	0.000	35.29 ± 6.90

* The measurements are repeated three times; dispersion evaluates through semi-dispersion.
§ The measurements are repeated ten times; dispersion evaluates through standard deviation.

Figure 6 shows a typical trend of the molar concentration of the compounds produced in 3 redox cycles using 7 minutes as reduction time. During the reduction steps, the gaseous mixture was mainly constituted by H_2, CO, CH_4, CO_2 and C_2H_4 traces. In the subsequent oxidation phase, pure H_2 was always achieved.
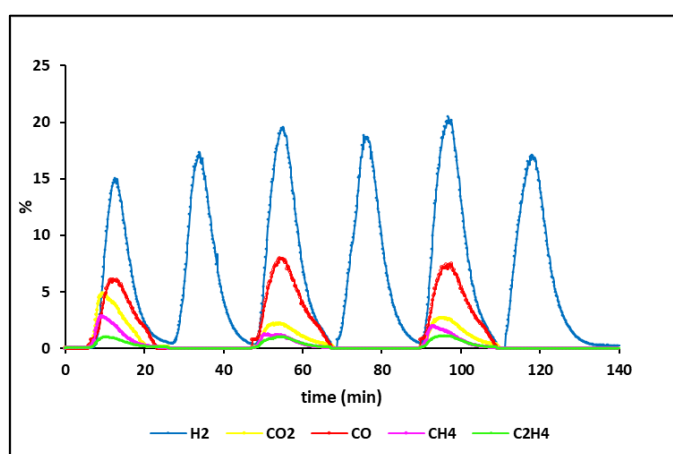

Fig. 6: Molar concentration of the gaseous species produced in the redox cycles (T=675 °C, P=1 atm, t_{red}=7 min).

Looking at figure 6, it should be noted that during the reduction step, the peak is reached at the end of the feeding period. On the contrary, in the oxidation step, the reaching of the hydrogen peak is independent of

the water feeding but depends only on the oxidation state of iron. The H_2 concentration goes to zero when iron particles are completely oxidized to Fe_3O_4.

In addition, in the first reduction, the areas of H_2 and CO peaks are smaller than that in the subsequent reduction peaks; this because the iron oxide at the beginning of the process is in the form of Fe_2O_3, which requires a higher amount of reducing agents to reach the metallic state (Fe^0) than that needed for magnetite. In fact, starting from the first oxidation peak, the restored iron oxide is magnetite.

3.3 *INFLUENCE OF MANGANESE DIOXIDE ADDITION IN THE PROCESS EFFICIENCY*

The tests carried out so far show that in the proposed configuration system, it is possible to produce pure H_2 but with low efficiency. The addition of a compound able to enhance the degree of reduction of the solid bed avoiding coke deposition can be one of the solutions to improve the H_2 production.

Tests were carried out, adding different quantities of MnO_2 powder (10 wt% and 40 wt% with respect to Fe_2O_3 weight) to investigate the effect of the amount of MnO_2 on the process efficiency.

The influence of MnO_2 addition was evaluated during three redox cycles. The amounts of H_2 produced in the oxidation step adding different amount of MnO_2 and in the presence of Fe_2O_3 alone are compared in figure 7 A; in all the oxidation peaks, the amounts of H_2, produced with MnO_2, were higher than those obtained using Fe_2O_3 alone. As shown in figure 7 B, with the addition of MnO_2, also the process efficiency was significantly improved at each oxidation cycle. From the comparison of the results obtained, the optimal amount of MnO_2 was individuated to be 10 wt%.
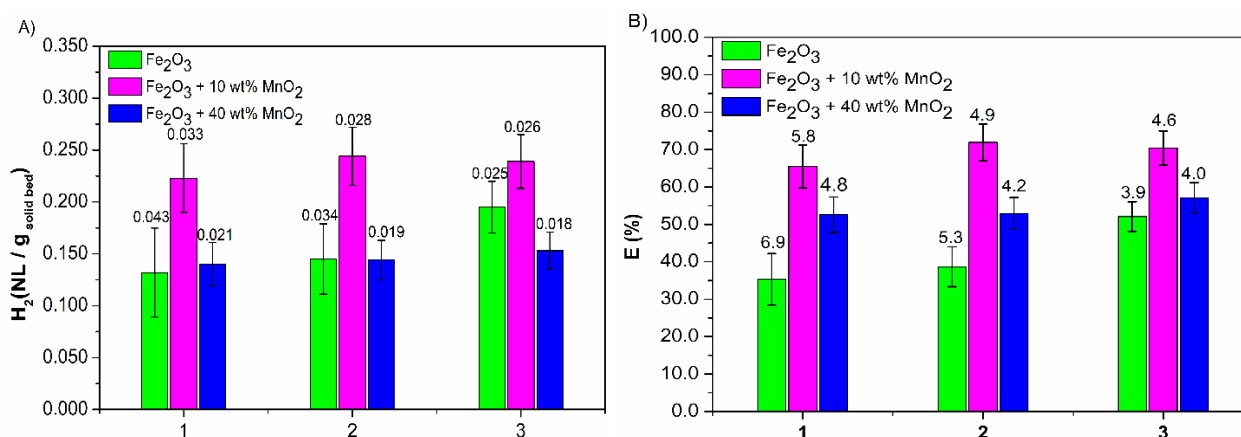

Fig 7: A) Hydrogen produced during three oxidation cycles with and without MnO_2; B) Process efficiency with and without the catalyst. The measurements are repeated ten times; dispersion evaluates through standard deviation.

In the tests with MnO_2, the theoretical produced H_2 calculations also include the amount of H_2 produced by the oxidation of MnO (equation 14). Accordingly, the efficiency was obtained by equation 22, considering the so calculated theoretical value of H_2. This comparison allows us to verify if MnO_2 is active, as hypothesized, in the iron oxide reduction or if it only works as iron in the oxidation reactions. According to the literature data, under the adopted operating conditions, MnO_2 can be reduced at MnO during the reduction step and subsequently re-oxidized to Mn_2O_3 in the oxidation phase [44]. Assuming that the whole amount of MnO_2 is reduced to MnO and then totally oxidized to Mn_2O_3, the hydrogen produced by this reaction should be equal to 0.021 L and 0.082 L for 10 wt% MnO_2 and 40 wt% of MnO_2, respectively. The difference between the H_2 produced with and without the addition of MnO_2 was calculated according to equation 23.

$$\Delta H_2 = H_{2e\,(Fe2O3+MnO2)} - H_{2e\,(Fe2O3)} \tag{23}$$

Moreover, according to fig. 7 A and 7 B, it is possible to evaluate that in the tests performed with the addition of MnO_2, the first and second peaks are more repeatable than the ones obtained only with Fe_2O_3. In particular, in these tests, a standard deviation of 0.01 L lower than the only hematite-based bed was

calculated. The third peaks for all the conditions present a higher standard deviation due to the incoming deactivation of the bed affecting the stability of the process.

As reported in table 4, ΔH_2 values were always higher than the maximum hydrogen produced by MnO oxidation, confirming that MnO_2 is not only a redox element but also improves the degree of the reduction of the iron oxides.

Table 4: ΔH_2 values and process efficiency for experiments with the addition of 10 wt% and 40 wt% of MnO_2.

N cycles	10 wt% MnO_2			40 wt% MnO_2		
	ΔH_2 (NL)		E (%)	ΔH_2 (NL)		E (%)
	Experimental	*Theoretical*		*Experimental*	*Theoretical*	
I cycle	0.179 ± 0.011	0.021	65.49 ± 5.76	0.103 ± 0.008	0.082	52.60 ± 4.76
II cycle	0.195 ± 0.004	0.021	71.91 ± 4.95	0.110 ± 0.007	0.082	52.94 ± 4.55
III cycle	0.103 ± 0.007	0.021	70.40 ± 5.28	0.084 ± 0.002	0.082	57.14 ± 4.85

The measurements are repeated ten times; dispersion evaluates through standard deviation.

Table 5 collects the main results of the steam iron process obtained by the literature and compares them with the results of this work. For each study, operating conditions, type of iron-based oxygen carrier, H_2 yields and H_2 purity are reported.

Table 5: Comparison between the H_2 yield, H_2 purity and CO concentration in the H_2 stream obtained with different iron based solid oxides available in the literature.

Solid bed	Reducing agent	Tests conditions	$H_{2\ yield\ max}$ (NL/g solid bed)	H_2 purity (%)	CO (ppm)	Ref
$Fe_2O_3/Al_2O_3/CeO_2$	Syngas	750 °C - 50 atm	0.159	NA	NA	[14]
$Fe_2O_3/Al_2O_3/CeO_2$	Ethanol	Red: 625 °C/700 °C - 1 atm Ox: 500 °C - 1 atm	0.276	NA	< 10	[37]
Iron ores	Syngas	750 °C /500 °C -1 atm	0.162	NA	< 50	[45]
Fe_2O_3 / m-ZrO_2	Syngas	600 °C - 1 atm	0.039	NA	NA	[46]
Fe_2O_3	H_2	700 °C / 900 °C -1 atm	0.044	NA	NA	[47]
Fe_2O_3	CO	780 °C - 1 atm	0.067	NA	< 25	[48]
Fe_2O_3	CO	900 °C - 1 atm	0.160	NA	NA	[49]
Fe_2O_3 composite particles	Syngas	830 °C - 1 atm	NA	99.80	NA	[20]
Fe_2O_3 + MnO_2	**Ethanol**	**675 °C - 1 atm**	**0.244**	**100.00**	**< 0.2**	**This work**

The data reported in Table 5 highlights the effectiveness of the reducing power of ethanol in the steam iron process. With ethanol, high hydrogen yield with high purity is produced at relatively low temperatures range (625 °C - 675 °C) and atmospheric pressure. Hydrogen yields comparable to those obtained in this study were reported only by Hormilleja et al. [37], which tested the steam iron process using ethanol as a reducing agent and $Fe_2O_3/Al_2O_3/CeO_2$ as redox solid bed. In the present work, however, the hydrogen stream is pure since coke deposition is avoided in the reduction step due to the optimization of the reduction duration and the addition of MnO_2.

In order to understand what is the role of MnO_x in the process, the amount of the gaseous species produced during the reduction step in three redox cycle with the addition of 10 wt% MnO_2 and in the presence of Fe_2O_3 alone are compared (figure 8). As shown in figures 8 A and 8 B, no significant differences in the amount of H_2

and CO are relieved; this result is unexpected because even in limited quantities also MnO_x consumes reducing agents in the reduction phase (equation 8-13). In contrast, the addition of MnO_2 resulted in a lower amount of CH_4 and a higher amount of CO_2 compared to the test performed with Fe_2O_3 alone (figure 8 C and 8 D). Finally, no differences are detected in the ethylene amount produced (figure 8 E).
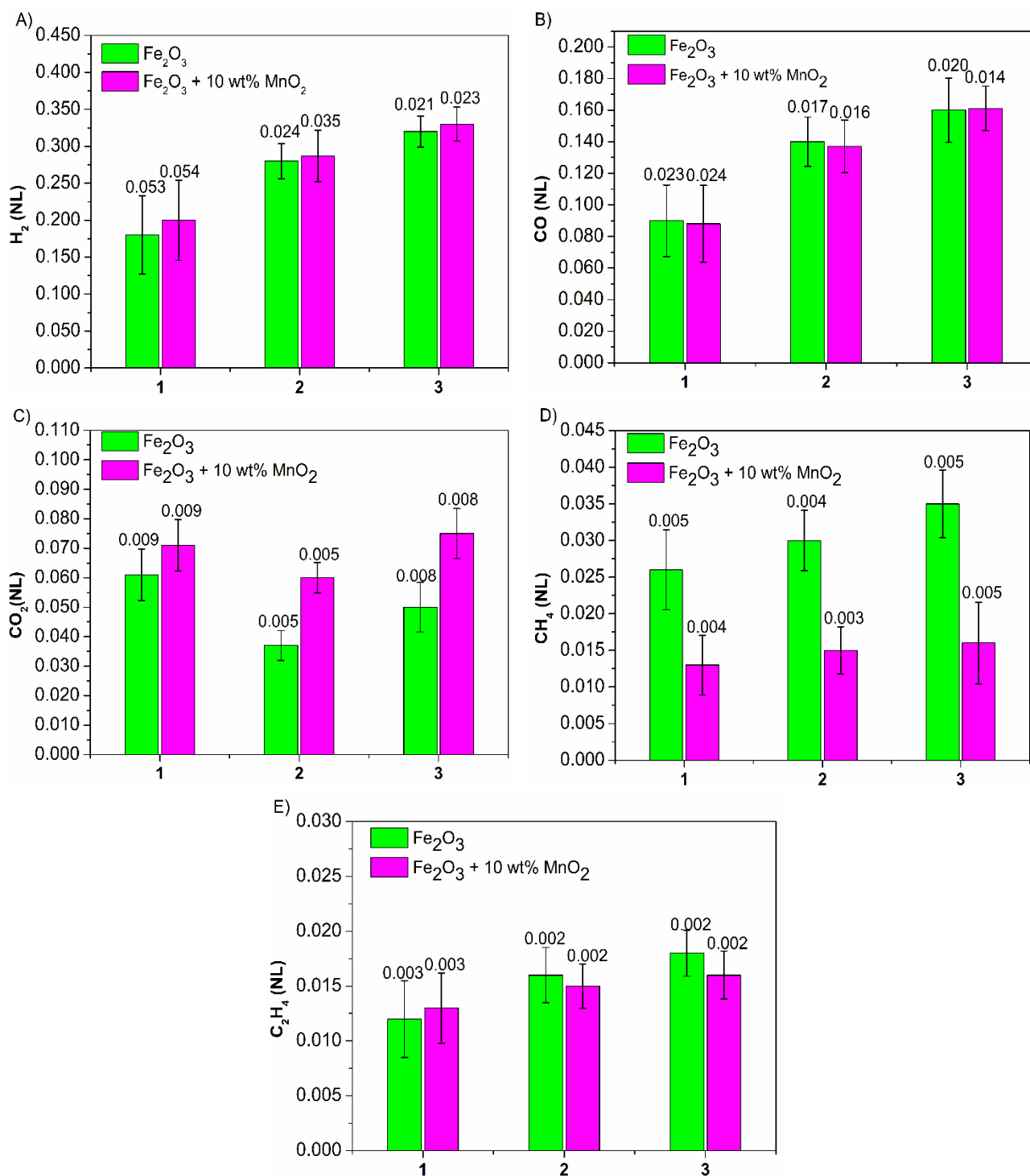

Fig 8: Comparison of the amount of the species produced during the reduction step for three redox cycle with and without 10 wt% of MnO_2. A) H_2; B) CO; C) CO_2; D)CH_4; E) C_2H_4. The measurements are repeated ten times; dispersion evaluates through standard deviation.

The results collected in figure 8 suggest that in the presence of MnO_x, the methane cracking reaction is enhanced. Several literature studies confirm that at high temperatures, also methane actively participates in the reduction of MnOx through reactions 17, 25 and 26 [50,51,32].

$$CH_4 \leftrightarrow C + 2H_2 \tag{17}$$
$$MnO_2 + C \leftrightarrow CO + MnO \tag{25}$$
$$MnO_2 + CH_4 \leftrightarrow MnO + CO + 2H_2 \tag{26}$$

As already described for the case of iron oxides, in the MnO_x reduction, a central role is played by the adsorbed active carbon resulting from methane cracking reaction (equation17); MnO_x are characterized by greater reticular oxygen mobility than that of iron oxides; the MnOx thus acts as oxygen donor during the reduction step enhancing the active carbon consumption (equation 25) [51]. The adsorbed carbon is oxidized to CO, obtaining the complete reduction of MnO_2 to MnO and additional syngas according to (equation 26) is produced [50]. As a consequence, the equilibrium methane cracking reaction is shifted to the right side with respect to the experiments carried out with the only Fe_2O_3; the additional carbon and hydrogen produced can reduce iron oxides according to the simplified scheme already proposed in figure 5.

From the results obtained, it can be concluded that the addition of MnO_2 improves the reduction grade of the bed enriching the gas phase in reducing compounds at the expense of methane and avoiding coke formation at this high grade of reduction too. As shown in figure 8 C, a better reduction of the bed is also confirmed by a higher quantity of CO_2 outgoing.

The proposed role of MnO_2 on the process can also explain why an increased amount of MnO_2 (40 wt%) decreases the overall process efficiency. In fact, CH_4 is already consumed when 10 % of MnO_2 is used, in the case of a higher amount of CH_4 is available for the reduction of MnO_2 and thus, only a small amount of MnO_2 is reduced with the active carbon resulting from the methane cracking reaction, the remaining MnO_2 particles are reduced with syngas causing a worse reduction of the Fe. As a consequence, the overall amount of H_2 and CO are used to reduce not only the iron oxides but also the additional MnO_2, decreasing the synergic effect of the use of iron and manganese oxides.

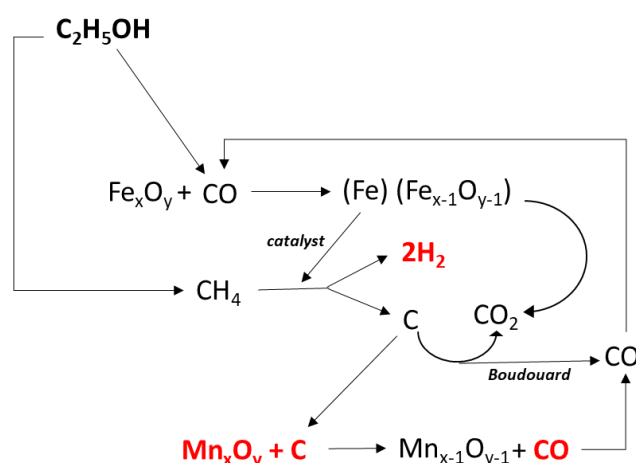The simplified scheme concerning the effect of MnOx addition in the iron oxides reduction is reported in Figure 9.

Fig 9: Effect of MnO_2 addition in iron oxides reduction with ethanol (675 °C, 1 atm).

3.4 STABILITY OF THE SYSTEM IN MULTIREDOX CYCLES

Currently, the research for metal oxides with high reactivity and stability is still the aim of several studies on the steam-iron process. An experiment with a high number of redox cycles (6 cycles) was conducted to verify

whether the powder mixture tested in this work present also good stability in terms of the production of pure hydrogen. The test was carried out at the optimal conditions previously identified (Fe_2O_3 + 10 wt% MnO_2).

Both the amounts of hydrogen obtained and the process efficiency related to each redox cycle are shown in table 6.

Table 6: Amounts of H_2 produced and process efficiency in 6 redox cycles. Solid bed: 1.59 g Fe_2O_3 + 0.16 g MnO_2

N cycles		H_2 (NL / $g_{solid\ bed}$)	E (%)
I	cycle*	0.222 ± 0.033	65.5 ± 5.8
II	cycle*	0.244 ± 0.028	71.9 ± 4.9
III	cycle*	0.239 ± 0.026	70.4 ± 4.6
IV	cycle§	0.229 ± 0.009	67.2 ± 1.7
V	cycle§	0.214 ± 0.010	63.9 ± 1.8
VI	cycle§	0.206 ± 0.007	60.5 ± 1.2

*The measurements are repeated ten times; dispersion evaluates through standard deviation.

§ The measurements are repeated three times; dispersion evaluates through semi-dispersion.

A growing trend of hydrogen produced up to the third cycle is observed, confirming that in every cycle, the complete reduction of the particles is not achieved; this condition is essential to ensure the high purity of the hydrogen obtained when ethanol is used as a reducing agent since only with lower reduction grade, the coke deposition ca be avoided. The results also show that the Fe_2O_3 and MnO_2 powders do not have high stability under the operating conditions adopted; the efficiency of the process decreases from the maximum value of 72.27% reached at the third cycle to 60.50% at the sixth cycle. This instability is highly likely to be found in agglomeration/sintering phenomena of Fe and Mn, which cause a reduction of the reactive surface of the bed [52]. As a result, a smaller amount of magnetite is reduced and therefore, a lower amount of Fe is oxidized. The instability of the powders used in this work suggests that the presence of inert porous support could be an effective solution to increase the reactive surface and thus to improve the process stability [53].

4. CONCLUSIONS

The feasibility of using renewable ethanol as a reducing agent in the steam-iron process was demonstrated. At the adopted operating conditions (T = 675 °C and P = 1 atm), ethanol is completely decomposed in a gaseous mixture mainly composed of H_2 and CO with high reducing activity. To successfully use ethanol as a reducing agent for the production of pure hydrogen, the correct evaluation of the ethanol feeding time is crucial. At the operating condition used in this work, an amount of ethanol equal to 5 $mmol_{C2H5OH}/g_{Fe2O3}$ (reduction time of 7 minutes) seems to be the optimal value to avoid coke formation leading, however, to a low degree of reduction of hematite and, therefore, poor process efficiency. The addition of MnO_2 has a dual function in the process: it produces additional hydrogen participating in the redox cycles and increases the amount of reducing gas, allowing a better reduction of the bed, avoiding coke deposition. The highest H_2 yields (0.244 ± 0.028 L) and process efficiency (71.9% ± 4.9%) were obtained, adding 10 wt% of MnO_2. Finally, the extended duration test (6 redox cycles) shows that the overall process efficiency decreases of 16.28% and, therefore, that the powders used are not sufficiently stable to be applied on the industrial scale. To reduce the uncertainty sources of the process, tests with a higher number of cycles should be carried out. For the first time, the synergic effect of MnO_2 and Fe_2O_3 was tested in the steam iron process allowing a doubled value of the efficiency, having anyway a pure hydrogen stream, ideal for PEMFC applications pure hydrogen stream, ideal for PEMFC applications.

List of abbreviations

PEMFCs	Proton-Exchange Membrane Fuel Cells
CLH	Chemical Looping Hydrogen
CLC	Chemical Looping Combustion
g $_{solid\ bed}$	Grams of the solid redox bed (Fe_2O_3 or $Fe_2O_3+MnO_2$)
E (%)	Percentage of the efficiency of the process
H_{2e}	The amount of hydrogen produced measured in normal liter
H_{2t}	Theoretical amount of hydrogen produced by the complete oxidation of the particles
ΔH_2	Difference between the amount of hydrogen produced with and without MnO_2

REFERENCES

1. Camara GA, Ticianelli EA, Mukerjee S, Lee SJ, McBreen J. The CO Poisoning Mechanism of the Hydrogen Oxidation Reaction in Proton Exchange Membrane Fuel Cells. *J Electrochem Soc*. 2002;149(6):A748. doi:10.1149/1.1473775

2. O'Brien CP, Lee IC. CO Poisoning and CO Hydrogenation on the Surface of Pd Hydrogen Separation Membranes. *J Phys Chem C*. 2017;121(31):16864-16871. doi:10.1021/acs.jpcc.7b05046

3. Wee JH. Applications of proton exchange membrane fuel cell systems. *Renew Sustain Energy Rev*. 2007;11(8):1720-1738. doi:10.1016/j.rser.2006.01.005

4. Global CO2 emissions in 2019 – Analysis - IEA. https://www.iea.org/articles/global-co2-emissions-in-2019. Accessed March 23, 2020.

5. Holladay JD, Hu J, King DL, Wang Y. An overview of hydrogen production technologies. *Catal Today*. 2009;139(4):244-260. doi:10.1016/j.cattod.2008.08.039

6. Sengodan S, Lan R, Humphreys J, et al. Advances in reforming and partial oxidation of hydrocarbons for hydrogen production and fuel cell applications. *Renew Sustain Energy Rev*. 2018;82(July 2016):761-780. doi:10.1016/j.rser.2017.09.071

7. Ruocco C, Palma V, Ricca A. Hydrogen production by oxidative reforming of ethanol in a fluidized bed reactor using a Pt[sbnd]Ni/CeO2[sbnd]SiO2 catalyst. *Int J Hydrogen Energy*. 2019. doi:10.1016/j.ijhydene.2018.12.154

8. Leal EM, Bastos-Netto D, Leal AM. Analysis of Hydrogen Production from Ethanol for Fuel Cell Applications. *Proc Ninth Asia-Pacific Int Symp Combust Energy Util*. 2008:41-47.

9. Shiva Kumar S, Himabindu V. Hydrogen production by PEM water electrolysis – A review. *Mater Sci Energy Technol*. 2019;2(3):442-454. doi:10.1016/j.mset.2019.03.002

10. Stojić DL, Marčeta MP, Sovilj SP, Miljanić ŠS. Hydrogen generation from water electrolysis - Possibilities of energy saving. In: *Journal of Power Sources*. Vol 118. Elsevier; 2003:315-319. doi:10.1016/S0378-7753(03)00077-6

11. Hacker V, Fankhauser R, Faleschini G, et al. Hydrogen production by steam-iron process. *J Power Sources*. 2000;86(1):531-535. doi:10.1016/S0378-7753(99)00458-9

12. Luo M, Yi Y, Wang S, et al. Review of hydrogen production using chemical-looping technology. *Renew Sustain Energy Rev*. 2018;81(July 2017):3186-3214. doi:10.1016/j.rser.2017.07.007

13. Rostrup-Nielsen JR. New aspects of syngas production and use. *Catal Today*. 2000;63(2-4):159-164. doi:10.1016/S0920-5861(00)00455-7

14. Voitic G, Nestl S, Malli K, et al. High purity pressurised hydrogen production from syngas by the steam-iron process. *RSC Adv*. 2016;6(58):53533-53541. doi:10.1039/c6ra06134f

15. Chiesa P, Lozza G, Malandrino A, Romano M, Piccolo V. Three-reactors chemical looping process for hydrogen production. *Int J Hydrogen Energy*. 2008;33(9):2233-2245. doi:10.1016/j.ijhydene.2008.02.032

16. Hormilleja E, Durán P, Plou J, Herguido J, Peña JA. Hydrogen from ethanol by steam iron process in fixed bed reactor. In: *International Journal of Hydrogen Energy*. Vol 39. ; 2014:5267-5273. doi:10.1016/j.ijhydene.2014.01.002

17. Yang JB, Cai NS, Li ZS. Hydrogen production from the steam-iron process with direct reduction of iron oxide by chemical looping combustion of coal char. *Energy and Fuels*. 2008;22(4):2570-2579. doi:10.1021/ef800014r

18. Bleeker MF, Kersten SRA, Veringa HJ. Pure hydrogen from pyrolysis oil using the steam-iron process. *Catal Today*. 2007;127(1-4):278-290. doi:10.1016/j.cattod.2007.04.011

19. Gupta P, Velazquez-Vargas LG, Fan LS. Syngas redox (SGR) process to produce hydrogen from coal derived syngas. *Energy and Fuels*. 2007;21(5):2900-2908. doi:10.1021/ef060512k

20. Li F, Kim HR, Sridhar D, et al. Syngas chemical looping gasification process: Oxygen carrier particle selection and performance. *Energy and Fuels*. 2009;23(8):4182-4189. doi:10.1021/ef900236x

21. Urasaki K, Tanimoto N, Hayashi T, Sekine Y, Kikuchi E, Matsukata M. Hydrogen production via steam-iron reaction using iron oxide modified with very small amounts of palladium and zirconia. *Appl Catal A Gen*. 2005;288(1-2):143-148. doi:10.1016/j.apcata.2005.04.023

22. Jin GT, Ryu HJ, Jo SH, Lee SY, Son SR, Kim SD. Hydrogen production in fluidized bed by chemical-looping cycle. *Korean J Chem Eng*. 2007;24(3):542-546. doi:10.1007/s11814-007-0096-5

23. Galvita V, Sundmacher K. Hydrogen production from methane by steam reforming in a periodically operated two-layer catalytic reactor. *Appl Catal A Gen*. 2005;289(2):121-127. doi:10.1016/j.apcata.2005.04.053

24. Lin Y, Tanaka S. Ethanol fermentation from biomass resources: Current state and prospects. *Appl Microbiol Biotechnol*. 2006;69(6):627-642. doi:10.1007/s00253-005-0229-x

25. Biofuels, from ethanol to biodiesel, facts and information. https://www.nationalgeographic.com/environment/global-warming/biofuel/. Accessed March 26, 2020.

26. Sivaramakrishnan R, Su MC, Michael J V., Klippenstein SJ, Harding LB, Ruscic B. Rate constants for the thermal decomposition of ethanol and its bimolecular reactions with OH and D: Reflected shock tube and theoretical studies. *J Phys Chem A*. 2010;114(35):9425-9439. doi:10.1021/jp104759d

27. Park J, Zhu RS, Lin MC. *Thermal Decomposition of Ethanol. 1. Ab Initio MO/RRKM Prediction of Rate Constant and Product Branching Ratios*.

28. Luo J, Zhang Q, Garcia-Martinez J, Suib SL. Adsorptive and acidic properties, reversible lattice oxygen evolution, and catalytic mechanism of cryptomelane-type manganese oxides as oxidation catalysts. *J Am Chem Soc*. 2008;130(10):3198-3207. doi:10.1021/ja077706e

29. Delimaris D, Ioannides T. Intrinsic activity of MnOx-CeO2 catalysts in ethanol oxidation. *Catalysts*. 2017;7(11). doi:10.3390/catal7110339

30. Peluso MA, Sambeth JE, Thomas HJ. COMPLETE OXIDATION OF ETHANOL OVER MnOx Miguel A. Peluso, Jorge E. Sambeth* and Horacio J. Thomas. *React Kinet Catal Lett*. 2003;80(2):241-248.

31. Ren TZ, Yuan ZY, Du GH, Su BL. Facile preparation of nanostructured manganese oxides by hydrotreatment of commercial particles. *Stud Surf Sci Catal*. 2006;162:425-432. doi:10.1016/S0167-2991(06)80936-5

32. Stobbe ER, De Boer BA, Geus JW. The reduction and oxidation behaviour of manganese oxides. *Catal Today*. 1999;47(1-4):161-167. doi:10.1016/S0920-5861(98)00296-X

33. Miller DD, Smith M, Shekhawat D. Interaction of manganese with aluminosilicate support during high temperature (1100 °C) chemical looping combustion of the Fe-Mn-based oxygen carrier. *Fuel*. 2020;263:116738. doi:10.1016/j.fuel.2019.116738

34. ROSS HU. The Fundamental Aspects of iron ores reduction. *SSRN Electron J*. 2012:134-142. doi:10.2139/ssrn.2176050

35. Sesen FE. Practical reduction of manganese oxide. *J Chem Technol Appl*. 2017;01(01):3-4. doi:10.35841/chemical-technology.1.1.26-27

36. Pashchenko D. Flow dynamic in a packed bed filled with Ni-Al2O3 porous catalyst: Experimental and numerical approach. *AIChE J*. 2019;65(5):e16558. doi:10.1002/aic.16558

37. Hormilleja E, Durán P, Plou J, Herguido J, Peña JA. Hydrogen from ethanol by steam iron process in fixed bed reactor. *Int J Hydrogen Energy*. 2014;39(10):5267-5273. doi:10.1016/j.ijhydene.2014.01.002

38. Dunker AM, Kumar S, Mulawa PA. Production of hydrogen by thermal decomposition of methane in a fluidized-bed reactor - Effects of catalyst, temperature, and residence time. *Int J Hydrogen Energy*. 2006;31(4):473-484. doi:10.1016/j.ijhydene.2005.04.023

39. Wang Z, Fan W, Zhang G, Dong S. Exergy analysis of methane cracking thermally coupled with chemical looping combustion for hydrogen production. *Appl Energy*. 2016;168:1-12. doi:10.1016/j.apenergy.2016.01.076

40. Montero C, Remiro A, Valle B, Oar-Arteta L, Bilbao J, Gayubo AG. Origin and Nature of Coke in Ethanol Steam Reforming and Its Role in Deactivation of Ni/La2O3-αAl2O3 Catalyst. *Ind Eng Chem Res*. 2019;58(32):14736-14751. doi:10.1021/acs.iecr.9b02880

41. Hou T, Zhang S, Chen Y, Wang D, Cai W. Hydrogen production from ethanol reforming: Catalysts and reaction mechanism. *Renew Sustain Energy Rev*. 2015;44:132-148. doi:10.1016/j.rser.2014.12.023

42. Ibrahim AA, Fakeeha AH, Al-Fatesh AS, Abasaeed AE, Khan WU. Methane decomposition over iron catalyst for hydrogen production. *Int J Hydrogen Energy*. 2015;40(24):7593-7600. doi:10.1016/j.ijhydene.2014.10.058

43. Wang H, Li G, Ma J, Zhao D. The effect of methane decomposition on the formation and magnetic properties of iron carbide prepared from oolitic hematite. *RSC Adv*. 2017;7(7):3921-3927. doi:10.1039/c6ra26166c

44. Lin H, Chen D, Liu H, Zou X, Chen T. Effect of MnO2 crystalline structure on the catalytic oxidation of formaldehyde. *Aerosol Air Qual Res*. 2017;17(4):1011-1020. doi:10.4209/aaqr.2017.01.0013

45. Lachén J, Plou J, Durán P, Herguido J, Peña JA. Iron oxide ores as carriers for the production of high purity hydrogen from biogas by steam–iron process. *Int J Hydrogen Energy*. 2017;42(19):13607-13616. doi:10.1016/j.ijhydene.2016.11.152

46. Scheffe JR, Allendorf MD, Coker EN, Jacobs BW, McDaniel AH, Weimer AW. Hydrogen Production via Chemical Looping Redox Cycles Using Atomic Layer Deposition-Synthesized Iron Oxide and Cobalt Ferrites. *Chem Mater*. 2011;23:58. doi:10.1021/cm103622e

47. Wang Y, Wang X, Hua X, Zhao C, Wang W. The reduction mechanism and kinetics of Fe2O3 by hydrogen for chemical-looping hydrogen generation. *J Therm Anal Calorim*. 2017;129(3):1831-1838. doi:10.1007/s10973-017-6267-7

48. Bohn CD, Müller CR, Cleeton JP, et al. Production of very pure hydrogen with simultaneous capture

of carbon dioxide using the redox reactions of iron oxides in packed beds. *Ind Eng Chem Res*. 2008;47(20):7623-7630. doi:10.1021/ie800335j

49.   Chen S, Xiang W, Xue Z, Sun X. Experimental investigation of chemical looping hydrogen generation using iron oxides in a batch fluidized bed. *Proc Combust Inst*. 2011;33(2):2691-2699. doi:10.1016/j.proci.2010.08.010

50.   Alizadeh R, Jamshidi E, Zhang G. Transformation of methane to synthesis gas over metal oxides without using catalyst. *J Nat Gas Chem*. 2009;18(2):124-130. doi:10.1016/S1003-9953(08)60105-X

51.   Anacleto N, Ostrovski O, Ganguly S. Reduction of manganese oxides by methane-containing gas. *ISIJ Int*. 2004;44(9):1480-1487. doi:10.2355/isijinternational.44.1480

52.   Zhong Y, Gao J, Wang Z, Guo Z. Influence of particle size distribution on agglomeration/ defluidization of iron powders at elevated temperature. *ISIJ Int*. 2017;57(4):649-655. doi:10.2355/isijinternational.ISIJINT-2016-487

53.   Fang H, Haibin L, Zengli Z. Advancements in development of chemical-looping combustion: A review. *Int J Chem Eng*. 2009;2009(ii). doi:10.1155/2009/710515